Quantitatively analysis of nonlinear/linear nanofocusing of plasmonic tips array driven via radial vector beam

Donghui Bai,[1,4] Lu Zhang,[1,4] Chao Meng,[1] Lei Xu,[2,5] Feng Gao,[3] and Wending Zhang[1,*]

[1]MOE Key Laboratory of Material Physics and Chemistry under Extraordinary Conditions and Shaanxi Key Laboratory of Optical Information Technology, School of Physics and Technology, Northwestern Polytechnical University, Xi'an 710129, China
[2]Advanced Optics & Photonics Laboratory, Department of Engineering, School of Science & Technology, Nottingham Trent University, Nottingham NG11 8NS, United Kingdom
[3]MOE Key Laboratory of Weak-Light Nonlinear Photonics, TEDA Applied Physics Institute and School of Physics, Nankai University, Tianjin 300457, China
[4]The authors contributed equally to this work.
[5]lei.xu@ntu.ac.uk
**zhangwd@nwpu.edu.cn*

Abstract:
Electric field enhancement of the plasmonic tip-based nanofocusing light field determines the interaction efficiency of light and matter. Herein, the nonlinear/liner nanofocusing of the plasmonic tips array (PTA) is quantitatively analyzed, under excitation of the radial vector beam (RVB) and the linear polarization beam (LPB), respectively. Second harmonic (SH) emission intensity of PTA, under ultrafast RVB excitation, has been increased 18.6 times than that of the ultrafast LPB excitation. Experimental result is coincided with the theoretical prediction of 20.5 times, revealing that PTA has better nonlinear nanofocusing under excitation of the ultrafast RVB. The linear nanofocusing is examined via surface-enhanced Raman scattering (SERS). Under continuous wave RVB excitation, Raman scattering intensity of 4-Mercaptobenzoic acid (4MBA) is increased 4.5 times than that of LPB excitation, coinciding with the theoretically calculated electric field intensity enhancement of 4.8 times. Furthermore, the linear nanofocusing of PTA is examined using Raman scattering of the monolayer graphene, revealing that the linear nanofocusing of PTA will be slightly deteriorated, when a monolayer graphene is coated on PTA. This method may be adopted as a plasmonic tip-based nanofocusing light field with significant electric field enhancement to increase the light-matter nonlinear/linear interaction efficiency.

Keywords:
Nonlinear plasmonic, Second harmonic, Nonlinear optics at surface, Local surface plasmon resonance, Self-assembly method, Surface-enhanced Raman scattering.

Introduction

Metallic nanostructures, with excellently localized surface plasmon resonance (LSPR) effect [1-3], have received widespread attention. Plasmonic tip is one of the typical metallic nanostructures [4]. Because the plasmonic tip-based nanofocusing light field has high electric field enhancement factor and small mode field volume, simultaneously, it has been used in the fields of attomolar DNA detection [5], single molecule Raman/fluorescence imaging [6, 7], nonlinear frequency conversion [8], hot-electron excitation [9], etc.

Nanofocusing characteristic of the plasmonic tip is determined by the longitudinal electric field component of the tightly focused excitation light, because only the electric field component perpendicular to the tip apex can effectively excite the surface plasmon mode near the tip apex [10]. Linear polarization beam (LPB) is generally used as the excitation source [11, 12]. However, because the tightly focused radial vector beam (RVB) has a stronger longitudinal electric field component than that of LPB [13], the plasmonic tip has a more significant electric field enhancement, when the tightly focused RVB is used as the excitation source. On the other hand, the linear and nonlinear nanofocusing of the plasmonic tip can be achieved, under illumination of the continuous wave (CW) and the ultrafast light [14], respectively. In case of excitation light with different polarization and time-domain characteristics, the linear and nonlinear plasmonic tip-based nanofocusing light field has been achieved, and then used for tip-enhanced nanospectroscopy [15, 16]. However, the electric field enhancement of the linear and nonlinear tip-based nanofocusing light field have not been quantitatively analyzed, under illumination of the excitation light with different polarization and time-domain characteristics.

Under excitation of the ultrafast pulse, the plasmonic tip-based nonlinear nanofocusing can be analyzed by its second-order nonlinear optical response [17, 18]. However, since the second-order nonlinear optical response of the plasmonic tip is very weak [19], the examination of the resultant second harmonic (SH) is very difficult. Therefore, under excitation of the ultrafast pulses with different polarizations, it is difficult to quantitatively analyze the tip-based nonlinear nanofocusing light field. The linear nanofocusing of the plasmonic tip can be quantitatively analyzed by Raman scattering intensity of the analytes excited via the tip-based linear nanofocusing light field. However, since Raman scattering cross section is very small [20], under excitation of a single plasmonic tip, Raman signal intensity of the analyte is very weak, so the quantitative analysis of the tip-based linear nanofocusing light field is also difficult to achieve. Plasmonic tips array (PTA) can amplify the nonlinear and linear optical response of the tip-based nanofocusing light field. However, when the plasmonic tips are located on the same horizontal plane, the gap mode may be generated between two adjacent plasmonic tips [21]. It will seriously affect the quantitative analysis of the plasmonic tip-based nanofocusing light field.

In this paper, we have quantitatively analyzed the nonlinear and liner nanofocusing of PTA with 3D scaffold distribution, under axially excited via RVB and LPB. The SH emission intensity of PTA, under excitation of the ultrafast RVB, has been increased 18.6 times than that of the ultrafast LPB excitation. Examination result is coincided with the theoretical prediction of SH emission enhancement of 20.5 times, revealing that PTA has better nonlinear nanofocusing under the ultrafast RVB excitation. The linear nanofocusing is experimentally examined via surface-enhanced Raman

scattering (SERS). Under CW RVB excitation, Raman signal intensity of 4MBA is increased 4.5 times than that of LPB excitation, which is consistent with the theoretical calculation result of 4.8 times. Furthermore, the linear nanofocusing of PTA is examined using the monolayer graphene, revealing that the linear nanofocusing of the PTA will be slightly deteriorated, when the analyte is tightly coated on the surface of the PTA.

Method

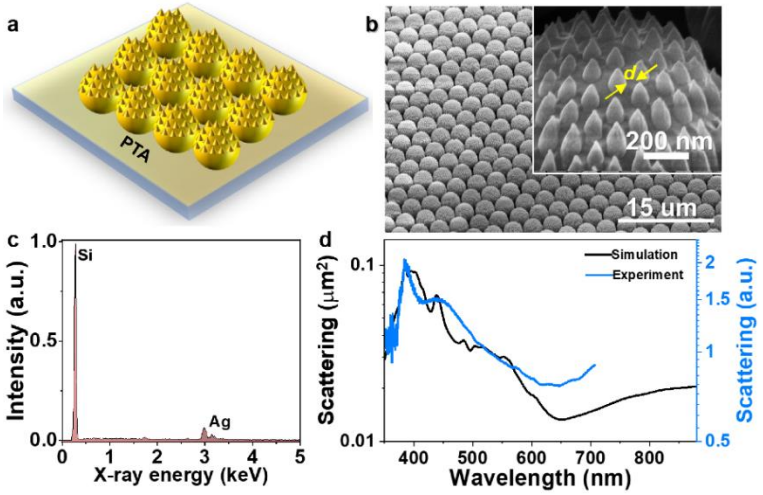

Fig. 1. (a) Sketch map of PTA with 3D scaffold distribution; (b) SEM image of PTA. The tip curvature radius is r=15 nm and the distanced between two adjacent tips is d=40 nm; (c) EDS spectrum of PTA; (d) Numerical simulation (red curve) and experimental measurement (blue curve) of the scattering spectra of PTA.

Figure 1(a) is schematic of PTA with 3D scaffold distribution, which is fabricated by combing self-assembled and the inductively couple plasma (ICP) etching technology. A monolayer-ordered hexagonally closed-packed polystyrene nanospheres (PS-NPs) with r=1.5 μm is formed on the silicon by the self-assembled method [22], and then the secondary self-assembly process is performed to form a monolayer-ordered hexagonally closed-packed PS-NPs with r=150 nm on the surface of PS-NPs with r=1.5 μm. The double-period PS-NPs array is etched using ICP for 90 seconds to form a nanocone array, and then an Ag film with thickness of 30 nm is deposited on the nanocone array via the electron beam evaporator. Figure 1(b) is the scanning electron microscope (SEM) image of the surface morphology of PTA with 3D scaffold distribution. The tip curvature radius is r=15 nm, and the distance between two adjacent tips is d=40 nm, as shown the inset of Fig. 1(b). According to the energy dispersive spectrum (EDS), as shown in Fig. 1(c), it can be known that the Ag film has been coated on the surface of the nanocone array. Thus, the PTA with curvature radius of r=15 nm has been prepared. More importantly, the PTA with 3D scaffold distribution can increase the distance between the adjacent tips to d=40 nm, thereby eliminating the influence of the gap mode, so as to ensure that only the surface mode near the tip apex can be excited. On this premise, it is possible to better compare the effects of the excitation light with different polarization distributions on the electric

field enhancement of the surface mode near the tip apex. It should be noted that although the tip curvature radius prepared in each batch will slightly fluctuate, the tip curvature radius prepared in the same batch can be basically uniform. Experimentally measured scattering spectrum of PTA within the wavelength range of 350 nm~700 nm is shown as the blue curve in Fig. 1(d), which is coincide with the simulated result, as shown the black curve in Fig. 1(d).

Results and discussions

The nonlinear and linear nanofocusing of the PTA is examined by using the second-order surface nonlinear optical response and SERS, which are only related to the electric field enhancement of the tip nanofocusing. Figure 2(a) is sketch map of the ultrafast pump pulse (ω) shinning on PTA. To facilitate theoretical simulation, only one plasmonic tip axially excited via the focused LPB and RVB is considered, as shown in Figs. 2(b) and 2(c), respectively. According to SEM image in Fig. 1(b), the tip curvature radius is set as r=15 nm. The 3D finite difference time domain (FDTD) method is used to simulate the electric field enhancement of the plasmonic tip [23-25]. The excitation wavelength is 810 nm, and the permittivity of Ag is obtained from Johnson and Christy [26]. The perfectly matched layers are used as absorption boundaries to simulate the plasmonic tip placed in an infinitely large free space. Based on the Richards-Wolf theory, the tightly focusing characteristics of the LPB and RVB are calculated in case of a micro-objective (MO) with NA=0.85, and the longitudinal electric field components of the tightly focused LPB and RVB are adopted to axially illuminate the plasmonic tip. Figures 2(d) and 2(e) are the electric field distributions near the tip apex, under axially excitation of LPB and RVB, respectively. As shown in Fig. 2(d), the electric field enhancement factor (L=$|E_{Tip}/E_{Incident}|$) is $L_{LPB}(\omega)$=3.1 under LPB excitation, and the surface mode is located on two sides of the tip apex. Under excitation of RVB, the electric field enhancement factor can reach $L_{RVB}(\omega)$=6.6, which is ~2.1 times that of LPB excitation. Furthermore, the surface mode is localized near the tip apex, as shown in Fig. 2(e).

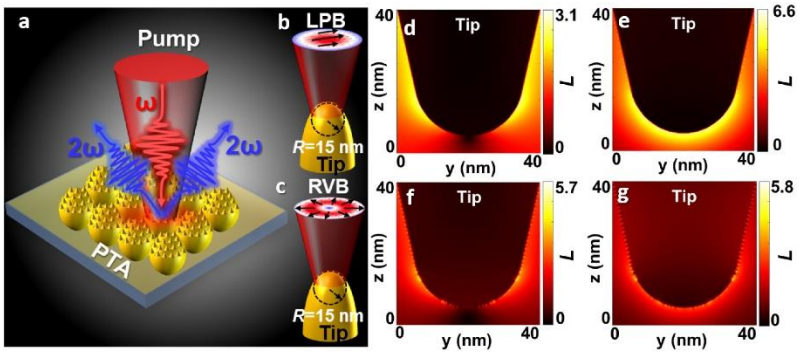

Fig. 2. (a) Sketch map of the ultrafast pump pulse (ω) shinning on the PTA; The focused ultrafast LPB (b) and RVB (c) shining on one plasmonic tip; (d) and (e) Electric field distributions near the tip apex corresponding to (b) and (c), respectively; Electric field distributions of SH (2ω) near the tip apex excited via LPB (f) and RVB (g), respectively.

Similarly, the electric field enhancement characteristic of the second harmonic (SH, 2ω) is also simulated. Figures 2(f) and 2(g) are the electric field distributions of SH

near the tip apex, under axially excitation of LPB and RVB, respectively. Note that the SH has significant electric field enhancement under excitation of LPB and RVB, but it has the same electric field enhancement factor of $L_{\mathrm{LPB}}(2\omega) \approx L_{\mathrm{RVB}}(2\omega) \approx 5.7$. Because the plasmonic tip has the optimal LSPR effect in the ultraviolet band, the polarization of the excitation light has no obvious effect on the electric field enhancement of SH.

The second-order polarization $P_{\perp,i}^{(2)}(2\omega)$ of the plasmonic tip can be expressed as [27, 28]

$$P_{\perp,i}^{(2)}(2\omega) \propto \chi_{\perp\perp\perp}^{(2)} L_i(2\omega) L_i^2(\omega) E_{\perp,i}(\omega) E_{\perp,i}(\omega) \tag{1}$$

where $\chi_{\perp\perp\perp}^{(2)}$ is the strongest component of the nonlinear surface susceptibility of the plasmonic tip, $L_i(\omega)$ and $L_i(2\omega)$ are the electric field enhancement factors for the pump light and SH, respectively. $E_{\perp,i}(\omega)$ is the electric field component perpendicular to the surface of the tip apex. $\perp$ denotes the component normal to the tip apex. i=1, 2 represent LPB and RVB, respectively. Therefore, the intensity of SH can be written as

$$I_i(2\omega) \propto \left[P_{\perp,i}^{(2)}(2\omega)\right]^2 \tag{2}$$

Under excitation of the ultrafast LPB and RVB, the intensity ratio of SH can be expressed as

$$\frac{I_2(2\omega)}{I_1(2\omega)} = \left[\frac{L_2(2\omega)}{L_1(2\omega)}\right]^2 \left[\frac{L_2^2(\omega)}{L_1^2(\omega)}\right]^2 \tag{3}$$

From Eq. (3), it can be known that the intensity ratio of SH is $I_2(2\omega)/I_1(2\omega) \approx 20.5$, revealing that RVB excitation can increase SH emission intensity of the plasmonic tip by 20 times than that of LPB excitation.

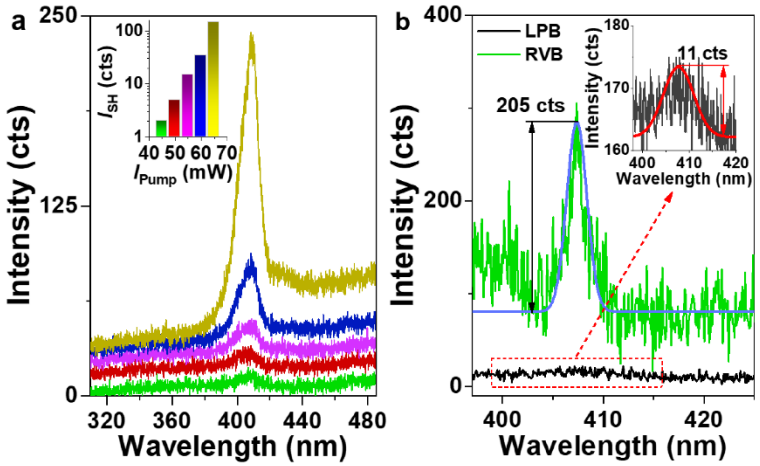

Fig. 3. (a) SH spectra of PTA axially excited via the ultrafast LPB, when the average power is P=45 mW, 50 mW, 55 mW, 60 mW, and 65 mW, respectively. Inset is the intensity dependence of SH on the pump pulse; (b) SH spectra of PTA axially excited via the ultrafast LPB (black curve) and RVB (green curve). Inset is the partial zoom SH spectrum (black curve) of PTA excited via the ultrafast LPB and Gaussian fit curve (red curve).

The nonlinear nanofocusing of PTA is experimentally examined by means of the second-order surface nonlinear optical response [29]. A femtosecond pulse (810 nm, 35 fs, 80 MHz) is used as the pump (ω) source. Figure 3(a) is the SH spectra, when PTA is axially illuminated via the ultrafast LPB. Note that SH spectra with central wavelength of 405 nm (2ω) are measured clearly, when the average pump power P=45 mW, and their intensity gradually increases as the pump power increases. As increase of the average pump power from 45 mW to 65 mW, the SH intensity increases from $I_{\mathrm{LPB}}(2\omega)$=2 counts (cts) to 154 cts, as shown in Fig. 3(a). Inset in Fig. 3(a) is the intensity dependence of the tip-emitted SH on the pump pulse. The nonlinear nanofocusing of PTA is furtherly compared, under excitation of the ultrafast LPB and RVB, respectively. The black curve in Fig. 3(b) is the SH spectrum of PTA excited via the ultrafast LPB with P=50 mW, and then SH intensity is examined to be $I_{\mathrm{LPB}}(2\omega)$=11 cts by Gaussian fit for SH spectrum, as shown the inset in Fig. 3(b). Keeping the average pump power constant and switching LPB to RVB via a vortex plate [10], the SH spectrum of PTA is measured, as shown the green curve in Fig. 3(b). Based on Gaussian fit, as shown the blue curve in Fig. 3(b), it can be known that SH intensity is $I_{\mathrm{RVB}}(2\omega)$=205 cts. The examination result proves that, under excitation of RVB, the SH emission intensity of the plasmonic tip is increased by $I_{\mathrm{RVB}}(2\omega)/I_{\mathrm{LPB}}(2\omega)$=18.6 times, which is coincide with the theoretical prediction of $I_2(2\omega)/I_1(2\omega)\approx$20.5.

Furthermore, the linear nanofocusing of PTA is examined using surface-enhanced Raman scattering (SERS). The 4-Mercaptobenzoic acid (4MBA) molecules is adopted to characterize the linear nanofocusing of PTA [30]. 15 μl of 4MBA with concentration of 10^{-5} M is transferred on PTA. Raman spectra of 4MBA under different excitation powers are measured. The excitation wavelength is 632.8 nm, and the integration time is 1 second. Figure 4(a) is Raman spectra of 4MBA excited via the CW LPB, when the excitation power is P=2 mW, 5 mW, 11 mW, 14 mW, and 17 mW, respectively. Figure 4(b) is the relationship between the Raman characteristic peak (1587 cm^{-1}) intensity and the excitation power. Note that the characteristic peak intensity has a linear response relationship with the excitation power, revealing that Raman signal intensity is linearly related to the electric field intensity of the excitation light. Figure 4(c) is the time stability mapping reconstituted with Raman spectrum of 4MBA within the time range of 100 seconds. Figure 4(d) is the histogram of Raman characteristic peak of 1578 cm^{-1}, with a relative standard deviation (RSD) of ~0.7% from the average Raman signal intensity. The time mapping result exhibits that the 4MBA molecules adsorbed on PTA has an excellent time stability, and reveal that the linear variation of Raman scattering intensity with the excitation power is reliable.

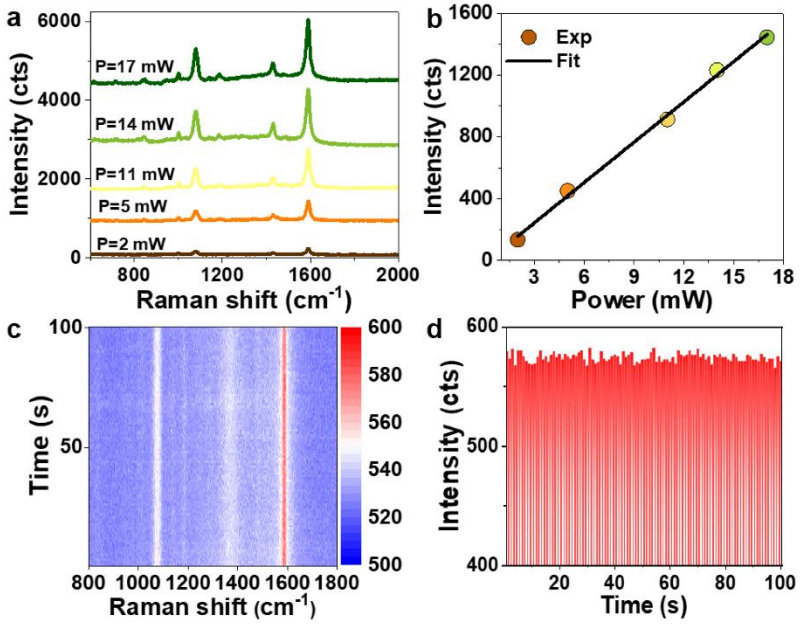

Fig. 4 (a) Raman spectra of 4MBA (10^{-5} M) deposited on PTA, which is excited by CW LPB with P=2 mW, 5 mW, 11 mW, 14 mW, and 17 mW, respectively; (b) Relationship between the Raman characteristic peak intensity and the excitation power; (c) Time stability mapping of the Raman spectra of 4MBA on PTA; (d) Intensity histogram of Raman characteristic peak (1578 cm^{-1}) of 4MBA within 100 seconds.

Figures 5(a) and 5(b) are the electric field distributions near the plasmonic tip apex, under axially excitation of LPB and RVB, respectively. The CW excitation light at 632.8 nm is focused on the tip apex via a MO with NA=0.85. As shown in Fig. 5(a), under excitation of LPB, the electric field enhancement factor is L_{LPB}=3.2. However, under excitation of RVB, as shown in Fig. 5(b), the electric field enhancement factor reaches to L_{RVB}=7, revealing that the electric field is increased $L_{RVB}/L_{LPB}\approx$2.2 times than that of LPB excitation. Figure 5(c) is Raman spectra of 4MBA absorbed on PTA and excited via the CW RVB and LPB, respectively. Under LPB excitation, the Raman scattering intensity is I_{LPB}^{Raman}=77 cts, as shown the black curve in Fig. 5(c). Keeping excitation power constant and switching LPB to RVB, the Raman scattering intensity can be increase to I_{RVB}^{Raman}=346 cts, as shown the blue curve in Fig. 5(c). Compared with LPB excitation, Raman scattering intensity of RVB excitation is increased by 4.5 times ($I_{RVB}^{Raman}/I_{LPB}^{Raman}\approx$4.5), which is coincide with the electric field intensity enhancement factor of $|L_{RVB}/L_{LPB}|^2\approx$4.8 under RVB excitation.

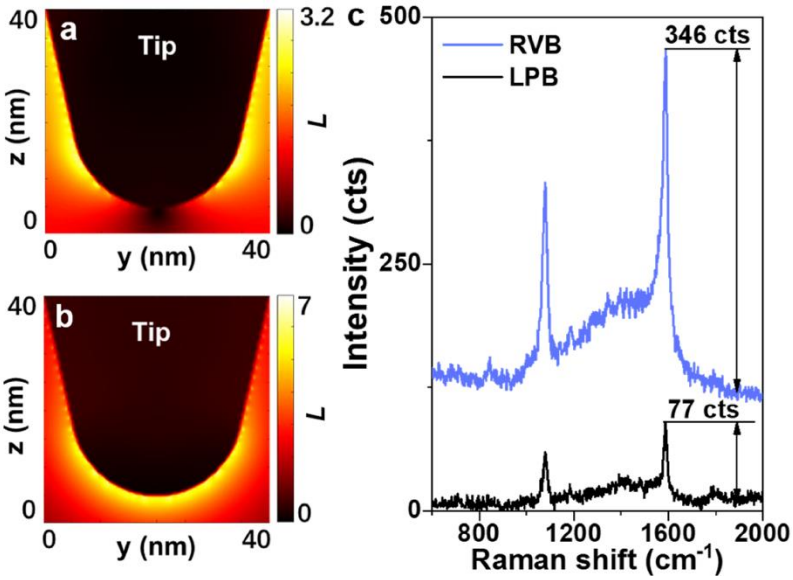

Fig. 5. Electric field distributions of the surface plasmon modes near a tip apex excited via the focused LPB (a) and RVB (b), respectively. (a) Raman spectra of 4MBA (10^{-5} M) deposited on PTA, and axially excited via the focused LPB (bule curve) and RVB (red curve), respectively.

Because the monolayer graphene is centrosymmetric material, the SH cannot be examined under ultrafast LPB and RVB excitations [31]. Therefore, only the linear nanofocusing of PTA is furtherly examined using the monolayer graphene. Figure 6(a) is the sketch map of the monolayer graphene laid flat on PTA, and the SEM image is shown in Fig. 6(c). Because of 3D scaffold distribution of PTA, when a monolayer graphene is laid flat on PTA, only part of the plasmonic tips can contact the monolayer graphene. Therefore, compared with LPB excitation, the SERS signal intensity of the monolayer graphene is not significantly enhanced under RVB excitation, which is only ~2.1 times that of LPB excitation, as shown in Fig. 6(e). Figure 6(b) is the sketch map of the monolayer graphene tightly coated on the surface of PTA, and Figure 6(d) is SEM image. The monolayer graphene is tightly coated on the surface of PTA, thus almost all the plasmonic tips can be in close contact with the monolayer graphene. SERS signal intensity obtained by RVB excitation is increased by ~3.7 times stronger than that of LPB excitation. According to the experimental results shown in Fig. 6, it can be known that the electric field enhancement of PTA is more significant under RVB excitation, when all the tip nanofocusing light fields interact with the analyte. However, since the analyte is in close contact with the PTA, it will degrade the nanofocusing characteristics of PTA.

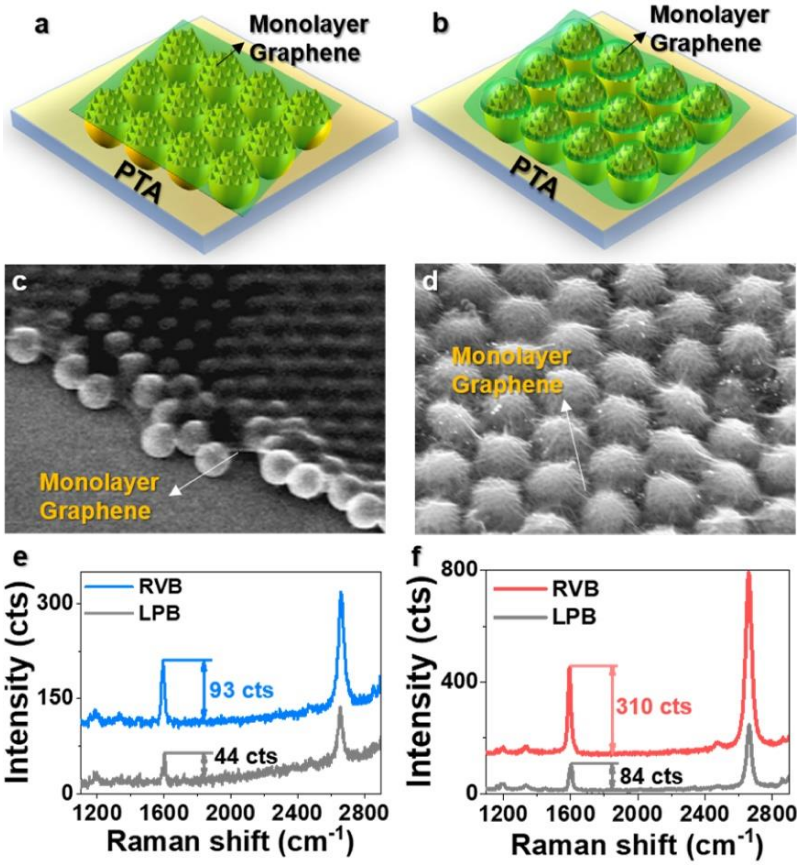

Fig. 6. Sketch maps of the monolayer graphene laid flat (a) and tightly coated (b) on the PTA, respectively; SEM images of the monolayer graphene laid flat (c) and tightly coated (d) on PTA, respectively; (e) Raman spectra of the monolayer graphene laid flat on PTA, excited via LPB (gray curve) and RVB (blue curve), respectively; (f) Raman spectra of the monolayer graphene tightly coated on PTA, excited via LPB (gray curve) and RVB (red curve), respectively.

Conclusions

In summary, we have quantitatively analyzed the nonlinear and liner nanofocusing of PTA axially excited via RVB and LPB, respectively. SH emission intensity, under ultrafast RVB excitation, has been increased ~18.6 times than that of the ultrafast LPB excitation. Examination result is coincided with the theoretical prediction of SH emission enhancement 20.5 times, revealing PTA has better nonlinear nanofocusing under ultrafast RVB excitation. The linear nanofocusing is examined with help of SERS method. Under CW RVB excitation, Raman signal intensity of 4MBA is increased 4.5 times than that of LPB, which is consistent with the theoretical calculation result of 4.8 times. Furthermore, the linear nanofocusing of PTA is examined by using monolayer graphene. Examination results prove that the nanofocusing of PTA will be slightly deteriorated, when a monolayer graphene is coated on PTA. The PTA may be used as a linear/nonlinear plasmonic nanofocusing light field with significant electric field enhancement to increase the linear/nonlinear light-matter interaction efficiency.

Acknowledgements

This work was financially supported by National Natural Science Foundation of China (NSFC) (11974282 and 91950207).

References

1. W. L. Barnes, A. Dereux, and T. W. Ebbesen, "Surface plasmon subwavelength optics," Nature vol. 424, no. 6950, pp. 824-830, 2003.
2. X. Lu, X. Zeng, H. Lv, Y. Han, Z. Mou, C. Liu, S. Wang, and S. Teng, "Polarization controllable plasmonic focusing based on nanometer holes, " Nanotechnology vol. 31, no. 13, pp.135201, 2020.
3. X. Luo, Extraordinary Young's Interferences and Super-Diffraction Laser Lithography[J]. Handbook of Laser Micro-and Nano-Engineering, Springer, Berlin, Germany 2020: 1-40.
4. M. I. Stockman, "Nanofocusing of optical energy in tapered plasmonic waveguides," Phys. Rev. Lett. vol. 93, no. 13, pp. 137404, 2004.
5. F. D. Angelis, F. Gentile, F. Mecarini, G. Das, M. Moretti, P. Candeloro, M. L. Coluccio, G. Cojoc, A. Accardo, C. Liberale, R. P. Zaccaria, G. Perozziello, L. Tirinato, A. Toma, G. Cuda, R. Cingolani, and E. D. Fabrizio, "Breaking the diffusion limit with super-hydrophobic delivery of molecules to plasmonic nanofocusing SERS structures," Nat. Photonics vol. 5, no. 11, pp. 682–687, 2011.
6. J. Lee, K. Crampton, N. Tallarida, and V. Apkarian, "Visualizing vibrational normal modes of a single molecule with atomically confined light," Nature vol. 568, no. 7750, pp. 78–82 2019.
7. B. Yang, G. Chen, A. Ghafoor, Y. Zhang, Y. Zhang, Y. Zhang, Y. Luo, J. Yang, V. Sandoghdar, J. Aizpurua, Z. Dong, and J. G. Hou, "Sub-nanometre resolution in single-molecule photoluminescence imaging," Nat. Photonics vol. 14, no. 11, pp. 693–699, 2020.
8. T. Jiang, V. Kravtsov, M. Tokman, A. Belyanin, and M. Raschke, "Ultrafast coherent nonlinear nanooptics and nanoimaging of graphene," Nat. Nanotechnol. vol. 14, no. 9, pp. 838-843, 2019.
9. A. Giugni, B. Torre, A. Toma, M. Francardi, M. Malerba, A. Alabastri, R. Proietti Zaccaria, M. I. Stockman, and E. D. Fabrizio, "Hot-electron nanoscopy using adiabatic compression of surface plasmons," Nat. Nanotechnol. vol. 8, no. 11, pp. 845-852, 2013.
10. W. Zhang, T. Xue, F. Lu, L. Zhang, C. Meng, J. Wang, T. Mei, "Second-order surface optical nonlinear response of plasmonic tip axially excited via ultrafast vector beams," Appl. Phys. Express vol. 13, no. 3, pp. 032002, 2020.
11. X. Luo, D. Tsai, M. Gu, and M. Hong, "Extraordinary optical fields in nanostructures: from sub-diffraction-limited optics to sensing and energy conversion," Chem. Soc. Rev. vol. 48, no. 8, pp. 2458-2494, 2019,
12. L. Chen, Y. Zhou, Y. Li, and M. Hong, "Microsphere enhanced optical imaging and patterning: From physics to applications featured," Appl. Phys. Rev. vol. 6, no. 2, pp. 021304, 2019.
13. K. S. Youngworth and T. G. Brown, "Focusing of high numerical aperture cylindrical-vector beams," Opt. Express vol. 7, no. 2, pp. 77–87, 2000.
14. W. Zhang, L. Zhang, F. Lu, D. Bai, T. Xue, C. Meng, M. Liu, D. Mao, F. Gao, and T. Mei, "Plasmon-enhanced nonlinear nanofocusing of gold nanoprisms driven via ultrafast azimuthal vector beam," Nanoscale vol. 12, no. 13, pp. 7045-7050, 2020.
15. S. Kim, N. Yu, X. Ma, Y. Zhu, Q. Liu, M. Liu, and R. Yan, "High external-efficiency nanofocusing for lens-free near-field optical nanoscopy," Nat. Photonics vol. 13, no. 9, pp. 636-643, 2019.
16. T. Umakoshi, M. Tanaka, Y. Saito, and P. Verma, "White nanolight source for optical nanoimaging," Sci. Adv. vol. 6, no. 23, pp. eaba4179, 2020.
17. X. S. Berweger, J. Atkin, X. Xu, R. Olmon, and M. Raschke, "Femtosecond nanofocusing with full optical waveform control," Nano Lett. vol.11, no. 10, pp. 4309–4313, 2011.

18. A. Bouhelier, M. Beversluis, A. Hartschuh, and L. Novotny, "Near-field second-harmonic generation induced by local field enhancement," Phys. Rev. Lett. vol. 90, no. 1, pp. 013903 2003.
19. Y. R. Shen, "Surface properties probed by second-harmonic and sum-frequency generation," Nature vol. 337, no. 6207, pp. 519–525, 1989.
20. A. Campion, and P. Kambhampati, "Surface-enhanced Raman scattering," Chem. Soc. Rev. vol. 27, no. 4, pp. 241-250, 1998.
21. Y. S. Hu, J. Jeon, T. J. Seok, S. Lee, Jason H. Hafner, R. A. Drezek, and H. Choo, "Enhanced Raman scattering from nanoparticle-decorated nanoconesubstrates: a practical approach to harness in-plane excitation," ACS Nano vol. 4, no. 10, pp. 5721–5730, 2010.
22. C. Hsu, S. Connor, X. Tang, and Y. Cui, "Wafer-scale silicon nanopillars and nanocones by Langmuir-Blodgett assembly and etching," Appl. Phys. Lett. vol. 93, no. 13, pp. 133109, 2008.
23. L. Zhang, W. Zhang, F. Lu, Z. Yang, T. Xue, M. Liu, C. Meng, P. Li, D. Mao, T. Mei, and J. Zhao, "Azimuthal vector beam exciting silver triangular nanoprisms for increasing performance of surface enhanced Raman spectroscopy," Photonics Res. vol.7, no. 12, pp. 1447-1453, 2019.
24. F. Lu, W. Zhang, L. Huang, S. Liang, D. Mao, F. Gao, T. Mei, and J. Zhao, "Mode evolution and nanofocusing of grating-coupled surface plasmon polaritons on metallic tip," Opto-Electronic Adv. vol.1, no.6, pp.180010, 2018.
25. Z. Li, W. Liu, Z. Li, H. Cheng, S. Chen, and J. Tian, "Fano-resonance-based mode-matching hybrid metasurface for enhanced second-harmonic generation," Opt. Lett. vol. 42, no. 16, pp. 3117-3120, 2017.
26. P. B. Johnson, and R. W. Christy, "Optical constants of the noble metals," Phys. Rev. B vol. 6, no. 12, pp. 4370-4379, 1972.
27. V. K. Valev, "Characterization of nanostructured plasmonic surfaces with second harmonic generation," Langmuir vol. 28, no. 44, pp. 15454−15471, 2012.
28. A. E. Minovich, A. E. Miroshnichenko, A. Y. Bykov, T. V. Murzina, D. N. Neshev, Y. S. Kivshar, "Functional and nonlinear optical metasurfaces," Laser Photonics Rev. vol. 9, no. 2, pp. 195-213, 2015.
29. L. Zhang, F. Lu, W. Zhang, K. Gao, T. Xue, M. Liu, D. Mao, L. Huang, F. Gao, and T. Mei, "Plasmon-enhanced linear and second-order surface nonlinear optical response of silver nanoparticles fabricated by using femtosecond pulse," Nanotechnology vol. 31, no. 3, pp. 035305, 2020.
30. Z. Yang, L. Meng, J. Lin, W. Yang, P. Radjenovic, S. Shen, Q. Xu, Z. Yang, Z. Tian, and J. Li, "3D hotspots platform for plasmon enhanced Raman and second harmonic generation spectroscopies and quantitative analysis," Adv. Optical Mater. vol. 7, no. 23, pp. 1901010, 2019.
31. Y. Zhang, D. Huang, Y. Shan, T. Jiang, Z. Zhang, K. Liu, L. Shi, J. Cheng, J. E. Sipe, W. Liu, and S. Wu, "Doping-induced second-harmonic generation in centrosymmetric graphene from quadrupole response," Phys. Rev. Lett. vol. 122, no.4, pp. 047401, 2019.